


Article

Application of the Tracer Test in a Hydrogeological Survey for a Pumped Storage Power Station

Wanlin Chen ¹, Jie Zhang ^{2,*}, Liqiang Chen ³, Kehan Miao ², Xiaosong Dong ²  and Yong Huang ²¹ Huadong Engineering (Fujian) Corporation Limited, Fuzhou 350003, China; chen_wl@hdec.com² School of Earth Sciences and Engineering, Hohai University, No. 1, Xikang Road, Nanjing 210098, China; miaokh2021@hhu.edu.cn (K.M.); dongxiaosong@hhu.edu.cn (X.D.); hyong@hhu.edu.cn (Y.H.)³ PowerChina Huadong Engineering Corporation Limited, Hangzhou 310014, China; chen_lq@ecidi.com

* Correspondence: zhang_jie@hhu.edu.cn; Tel.: +86-158-5063-9187

Abstract: In areas with complex hydrogeological conditions, the tracer test method is often used as an effective means in hydrogeological surveys. According to the results of tracer tests, hydrogeological parameters, including hydraulic gradient and permeability coefficient, fracture network leakage passages and their scale, and groundwater flow rate and direction can be quantitatively determined. This paper takes the upper reservoir of Yongxin Pumped Storage Power Station in Jiangxi Province as the research object, and focuses on the complex hydrogeological conditions of the upper reservoir. Three sets of tracer tests and multiple sets of single-hole flow rate and direction tests were conducted on the left and right banks of the reservoir and near surface gullies. The results showed that ZKS18 received tracers in all three tests, which indicates a close hydraulic connection between ZKS18 and the left bank, right bank, and surface gullies within the reservoir. Based on the single or multiple peak values of the tracer, it was determined that there are 1–6 leakage passages in the fractured rocks, with leakage passage sizes of 0.1–0.4 mm. According to the single-hole flow rate and flow direction tests, a self-developed instrument was used to determine the groundwater flow rate and flow direction at different depths in the test holes, which yielded results that were basically consistent with the results of the three-hole method. These results provide a basis for the use of tracer tests in hydrogeological surveys for water conservancy and hydropower engineering, and anti-seepage design of upper reservoirs.

Keywords: tracer test; hydrogeological survey; test of groundwater flow rate and direction; fractured rocks



Citation: Chen, W.; Zhang, J.; Chen, L.; Miao, K.; Dong, X.; Huang, Y. Application of the Tracer Test in a Hydrogeological Survey for a Pumped Storage Power Station. *Water* **2024**, *16*, 1100. <https://doi.org/10.3390/w16081100>

Academic Editor: Achim A. Beylich

Received: 4 March 2024

Revised: 31 March 2024

Accepted: 9 April 2024

Published: 11 April 2024



Copyright: © 2024 by the authors. Licensee MDPI, Basel, Switzerland. This article is an open access article distributed under the terms and conditions of the Creative Commons Attribution (CC BY) license (<https://creativecommons.org/licenses/by/4.0/>).

1. Introduction

Pumped storage power stations utilizing natural alpine basins face unique challenges due to their specific external conditions and functional designs, distinguishing from conventional river dams. In these settings, issues related to the seepage prevention of reservoir basin are more pronounced and necessitate stringent seepage control measures [1]. Leakage can prevent the reservoir from reaching its normal storage level, thereby impairing its functionality, diminishing the project's benefits, and potentially jeopardizing both production safety and public safety. This is particularly true for basins with inadequate seepage prevention capabilities, especially those characterized by karst formations and complex geological conditions. Consequently, the identification of leakage passages beneath the reservoir basin, assessment of the seepage pathways in fractured networks, analysis of the underground hydraulic connections, and the development of an effective seepage prevention strategy are critical for ensuring judicious investment management [2,3]. Comprehensive investigation of the complex hydrogeological conditions for the reservoir, determination of groundwater hydraulic connections, and identification of potential leakage passages are essential. These efforts provide a solid foundation for the hydrogeological surveys in water conservancy

and hydropower projects, and inform the design of effective seepage prevention measures for the reservoir [4].

The main methods of reservoir leakage detection include abnormal flow field analysis, borehole geophysical exploration, the seismic surface wave method, GIS, hydrochemical analysis, the tracer test, and other geophysical methods [5–11]. Among these, the groundwater tracer test represents a crucial methodology for elucidating flow systems, and is extensively applied in hydrogeological surveys and the identification of leakage within the hydraulic structures [12]. The tracer test is a detection method that places a source of material including solid particles, solutes, gases, and physical parameters like temperature and pressure [13], that can move with groundwater in a certain part of the groundwater system, and detect it at the expected location. Based on the detection results, the characteristics of the media and potential fields are comprehensively analyzed to obtain the hydrodynamic characteristics of the natural flow field of the groundwater system. By injecting tracers at the injection point and analyzing water samples at the reception point, hydrogeological parameters such as velocity of groundwater and permeability coefficient can be determined. The recharge, runoff, and discharge between the adjacent groundwater flow systems can be detected, and the location of groundwater watersheds and the connectivity, extension, and distribution of underground rivers can be determined. This helps in speculation about the relationship between groundwater and surface water, as well as the leakage pathways of the reservoir, which can provide a scientific basis for the division, resource evaluation, and pollution prevention of groundwater flow systems.

Lorenzi et al. [14] explored the flow pathways within karst systems using isotopic tracer tests and hydrogeochemical monitoring, subsequently developing a conceptual model that delineates spring recharge processes and demonstrates the overlay of karst networks upon regional base flows. Aquilanti et al. [15] employed DNA and fluorescein tracer tests to investigate the water cycle within the unsaturated zone in the Umbria-Marche limestone ridge and validated the efficacy of DNA tracers in such environments. Through a comprehensive analysis of multiple tracer test datasets, 3D seismic imagery, and well flow metrics, Bodin et al. [16] examined the karst conduit network employing a multi-path search algorithm, confirming their findings within the karst aquifer at the Hydrogeological Experimental Site (HES). Nanni et al. [17] utilized tracer tests to ascertain that the seismic events of 2016/2017 in central Italy enhanced the hydraulic conductivity of the basal aquifer, significantly altering groundwater circulation patterns. Martín-Rodríguez et al. [18] demonstrated how geometric factors, such as aquifer structure and the anisotropy of the drainage network, can skew the predominant drainage pathways within karst aquifers, as evidenced by dye tracer tests and response time disparities. Ren et al. [19] undertook a study on a complex karst aquifer in Southwest China, integrating multiple tracer tests, and chemical and isotope analyses, aiming for a rapid and effective method to pinpoint and identify pollution sources within intricate karst systems.

In recent years, the tracer technique has been gradually applied in the seepage detection of the reservoir dams. Qiu et al. [20] implemented an enhanced tracer test methodology, integrating both natural and artificial salt tracers, to quantitatively assess the leakage at Wanyao Dam, and conducted a detailed analysis of the leakage rate. Hua et al. [21] developed an innovative dimension reduction model (DRM) based on tracer test results, which effectively characterizes fractured networks and predicts the flow and transport within the fractured aquifers, further demonstrating its applicability to fractured network characterization at the field scale. Dogančić et al. [22] established the hydraulic connectivity between Shahneshin North and Dashtak North through the use of stable isotope analysis (δD and $\delta^{18}O$) alongside multiple tracer tests.

In the realm of water conservancy and hydropower engineering, accurately identifying the complex subterranean karst conduit systems, determining the seepage parameters of fractured rock masses, and pinpointing large-scale water-conducting fracture zones and leakage passages are critical for the design of the selection of anti-seepage strategies. Currently, the single-hole dilution method is predominantly applied in aquifer studies

but is seldom utilized in detecting leakage and quantifying groundwater parameters in dams and other hydraulic structures [23,24]. Furthermore, conservative tracer tests [25] are mainly employed to explore hydraulic connections within fracture networks and karst conduits, yet they often lack in-depth quantitative analysis. This paper introduces a novel quantitative approach for measuring the permeability parameters of rock masses and the dimensions of leakage passages via tracer tests. Additionally, it presents a new technique for assessing the flow rate and direction of groundwater in a single hole [26], which was successfully validated through engineering applications at the Yongxin Pumped Storage Power Station (YXPSPS). This method provides a solid foundation for future anti-seepage designs and seepage control measures.

2. Methods and Materials

2.1. Groundwater Flow Rate and Direction Tests in a Single Borehole

Radioisotopes are commonly used in the determination of groundwater flow rate and direction. This method has high accuracy. However, due to the potential risk of environmental pollution caused by isotopes, they are now rarely used. Therefore, this article develops a single-hole tracer test based on the salt tracer, which can quickly and conveniently obtain groundwater flow rate and direction.

(1) Determination of groundwater flow rate

Using the full-hole marking method, the salt tracer is injected into the borehole and diluted by stirring to evenly distribute the salt tracer throughout the entire borehole. Salt sinks and rises at a uniform rate, and the water column is vertically and uniformly marked. The electrical conductivity of the borehole is automatically monitored by instruments at different depths. Based on the attenuation rate of the salt tracer concentration at monitoring points and the variation pattern of the peak position, the methods of groundwater dynamics are applied to determine the direction of groundwater flow and the location of leakage passages. Without considering vertical flow, the concentration of tracer decreases with the groundwater movement, and its dilution rate is closely related to the groundwater flow rate, which is known as single-hole dilution method.

$$v_f = \frac{\pi r}{2At} \ln \frac{N_0}{N} \quad (1)$$

where v_f is the seepage velocity, and the relationship between groundwater seepage velocity, v_f , and actual flow rate, u , is $v_f = un$; n is porosity; r is the drilling radius; A is the correction coefficient for groundwater flow field distortion, generally taken as 0.5–2.0; N_0 is the initial concentration of tracer when t is equal to 0; N is the tracer concentration at different time t .

(2) Determination of groundwater flow direction

After injecting the tracer into the borehole, it will flow downstream with the groundwater in the aquifer, and its transport is related to factors such as groundwater flow rate, angle, and particle size around the borehole. Under the influence of these factors, the characteristic of tracer concentration is that the upstream direction is higher than the downstream direction, and other directions change sequentially. Therefore, tracer concentration can be measured around the well to determine the direction of groundwater flow based on the concentration relationship. Measurements can be conducted simultaneously in eight directions, and at the same time, the average conductivity data in each direction are recorded. Due to the smaller concentration of tracer in the downstream direction, according to the vector synthesis rule, the direction of groundwater flow can be obtained by synthesizing it. The test was conducted using a self-developed instrument (Hohai University, Nanjing, China) for determining the flow rate and direction of groundwater in a single hole. The device consists of 8 probes fixed at the north, south, east, and west, and their angle bisectors, and each probe has an angle difference of 45° (Figure 1). The data measured by each probe have high accuracy and have been compared with the data measured by the Canadian automatic recorder for the parameters, such as water level, water temperature,

and conductivity, with the number of Solinst Levellogger 5 LTC. The error between the two devices is less than one-thousandth, so the data measured by the self-developed instrument are reliable. During on-site testing, the tracer is first injected into the borehole, and then the device is fixed at a certain depth in the borehole to automatically collect conductivity data. These data can be stored and displayed in real time on the screen.

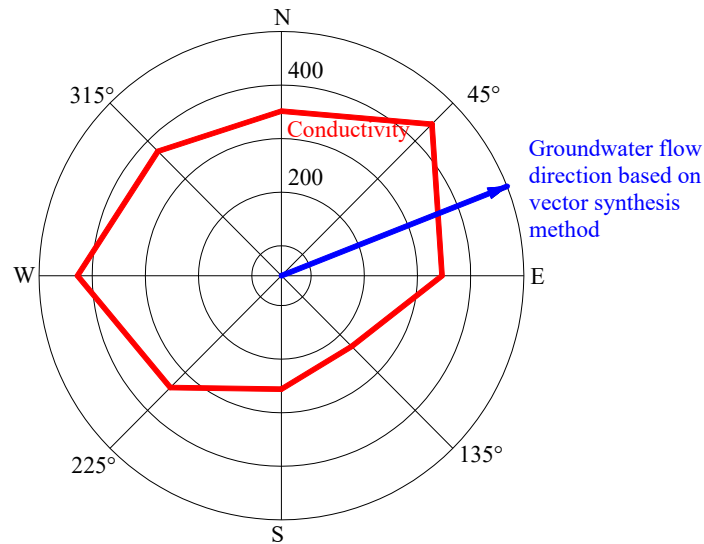


Figure 1. Vector synthesis method for groundwater flow direction.

2.2. Determination of Permeability Parameters of Fractured Rocks Based on Tracer Tests

There may be multiple different leakage passages between the tracer source and reception points, and the size of each passage is related to the fracture scale. Based on the abnormal values at the reception points in the on-site tracing test and the movement pattern of groundwater in the fractured water, the permeability coefficient of the fractured rocks and the size of the leakage passage can be estimated. The relevant formulas [27] can be expressed as:

$$J = \frac{\Delta H}{\Delta L} \quad (2)$$

$$u = \frac{\Delta L}{\Delta t} \quad (3)$$

$$K_f = \frac{u}{J} = \frac{gb^2}{12\mu} \quad (4)$$

$$Q = uA = K_fJA \quad (5)$$

$$T = K_fb \quad (6)$$

where J is the hydraulic gradient, ΔH is the water level difference between the injection and reception points, ΔL is the distance between two points, u is the actual average flow rate of groundwater, Δt is the time of groundwater movement, K_f is the fractured permeability coefficient, b is the fractured aperture, μ is the dynamic viscosity coefficient, Q is the actual groundwater flux, A is the cross-sectional area, and T is the transmissivity.

3. Case Study

3.1. Project Overview

The upper reservoir of Yongxin Pumped Storage Power Station (YXPSPS) is located in Gongyi Village, Aonan Town, Yongxin County, Ji'an City, Jiangxi Province, China. It is a valley-type reservoir constructed using a T-shaped valley formed by the intersection of Tongluoping and Daijiaoling Gullies with Yisong Gully. The Tongluoping Gully flows from northeast to southwest with a V-shaped valley and a longitudinal slope of about 5–10° at

the bottom. The ground elevation at the end of the reservoir is about 722 m. Daijiaoling Gully flows from southwest to northeast with a V-shaped valley and a longitudinal slope of about 5–10° at the bottom. The gully flows year-round, and the ground elevation at the end of the reservoir is about 707 m. The intersection of Tongluoping and Daijiaoling Gullies leads to the Yisonggou dam site area with a ground elevation of approximately 553 m.

The total installed capacity of YXPSPS is 1200 MW (4×300 MW). The power station is composed of the upper reservoir, lower reservoir, water conveyance system, underground power plant, and other buildings. After it is finished, it will supply power to the Jiangxi power grid and undertake tasks such as peak shaving, valley filling, energy storage, frequency regulation, phase regulation, and backup. It will play an important role in maintaining the safety, economy, and stable operation of the power grid. The normal water level of the upper reservoir is 646 m and the dead water level is 609 m. The regulating capacity of the reservoir is 10.92 million m^3 . The catchment area of the dam site is 1.37 km^2 .

The main structures of the upper reservoir include the asphalt concrete face rockfill dam, the stone material yard inside the reservoir, the anti-seepage of the reservoir basin, and the road on the reservoir bank. The dam type of the upper reservoir is an asphalt concrete face rockfill dam with a crest elevation of 649 m, a maximum dam height of 105.5 m, and a crest length of 360 m. The anti-seepage of the upper reservoir basin adopts a horizontal anti-seepage type. Except for the stone yard area inside the Daijiaoling Gully reservoir, the reservoir basin adopts the anti-seepage type of asphalt concrete panel around the reservoir and a geotextile membrane at the bottom of the reservoir (Figure 2).

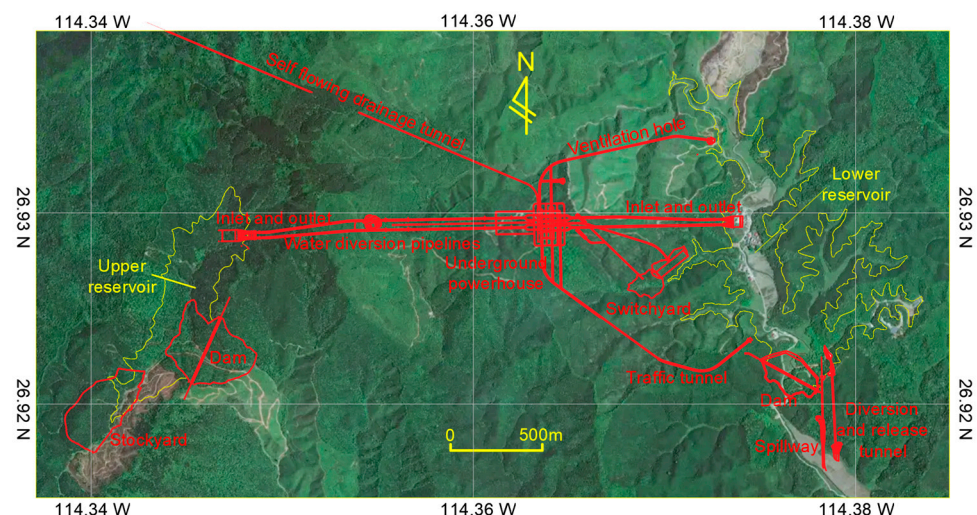


Figure 2. Layout of water conservancy project for YXPSPS.

3.2. Lithology

The lithology of the exposed strata in the engineering area is relatively complex. The bedrock mainly consists of metamorphic sandstone interbedded with slate in the Lower Paleozoic Cambrian (ϵ_1n), metamorphic sandstone interbedded with slate (ϵ_2gt , ϵ_3s^2), quartzite and quartz sandstone interbedded with a small amount of slate (ϵ_3s^3), metamorphic sandstone and quartz sandstone interbedded with slate (D_2t lower section) of the Upper Paleozoic Devonian (D), slate interbedded with metamorphic sandstone (D_2t upper section), calcareous sandstone and slate interbedded with metamorphic sandstone (D_2q middle lower section), metamorphic sandstone and calcareous sandstone interbedded with limestone (D_2q upper section), metamorphic sandstone interbedded with a small amount of sericite slate (D_3s), and quartz sandstone interbedded with slate (D_3x). The covering layer mainly consists of the residual slope layer (Q_4^{el+dl}), alluvial flood layer (Q_4^{al+pl}), colluvial slope layer (Q_4^{col+dl}), and artificial accumulation layer (Q_4s) of the Quaternary Holocene (Q_4) in the Cenozoic era (Figure 3).

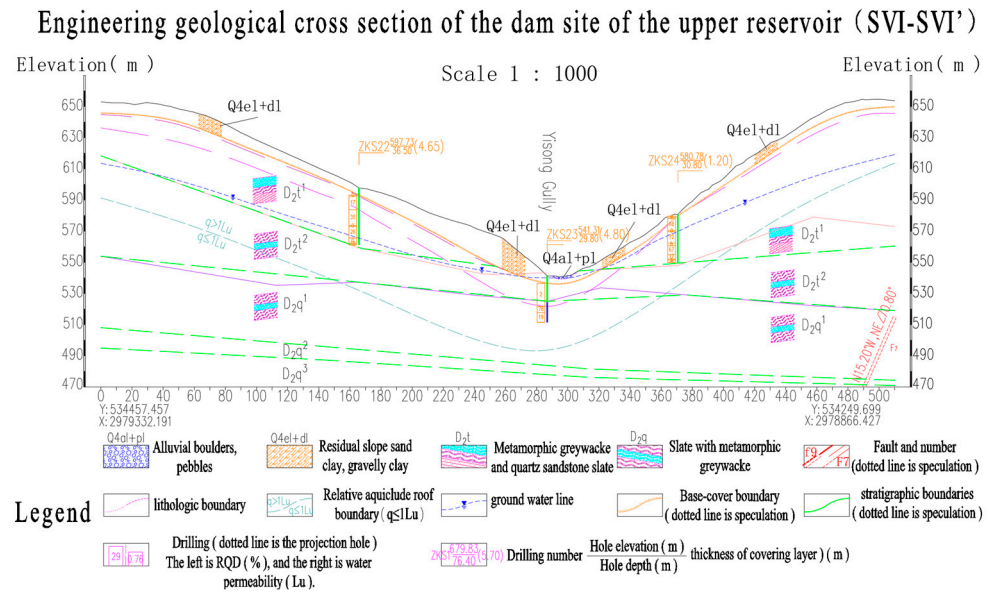


Figure 3. Engineering geological cross-section of the dam site of the upper reservoir (SVI-SVI').

3.3. Groundwater Types

According to the burial conditions and occurrence forms of groundwater, the types of groundwater in the engineering area can be divided into pore water, fracture water, and karst water. (i) Pore water is mainly distributed on the surface of the Quaternary cover layer and fully weathered layer, directly supplied by atmospheric precipitation, partially supplied by underlying bedrock fracture water, and discharged into low-lying terrain. The amount of water varies greatly due to seasonal influences. (ii) Fracture water is mainly distributed in bedrock joints, fractures, and fault zones, and is recharged by atmospheric precipitation and pore water. Its water-bearing capacity is mainly controlled by faults and fractures, and it is distributed in a vein and belt with significant spatial distribution differences and characteristics of non-uniformity and anisotropy. (iii) Karst water is distributed in carbonate rock layers, and there are three soluble rock bands (KRY1~KRY3) developed in the upper reservoir. The soluble rock bands are mainly calcareous sandstone with a small amount of limestone interlayers developed in deeper areas. Boreholes ZKS4 and ZKS57, and adit PD3, reveal karst caves. The water inrush phenomenon was found in boreholes ZKS4, ZKS18, ZKS57, and ZKS51, and adit PD3, in the dam site area. It is recharged by atmospheric precipitation, pore water, and fracture water, and the water-bearing capacity is mainly controlled by fractures, caves, and faults. It is distributed in a layer, vein, and belt, with significant spatial distribution differences and characteristics of non-uniformity and anisotropy. According to drilling data, the burial depth of groundwater in the dam axis of the upper reservoir is 59–91 m on the left bank, 0–3 m at the bottom of the gully, and 44–91 m on the right bank.

3.4. Process of the Tracer Tests

The tracer test was conducted from 29 April 2023 to 10 May 2023, with a total of three sets of tests. The injection source points were ZKS52, ZKS49, and ZKS50, respectively. There were a total of six reception points, namely ZKS18, ZKS49, ZKS51, ZKS55, ZKS56, and PD3. The location of the source and reception points is shown in Figure 4. The detailed test process is shown in Table 1.

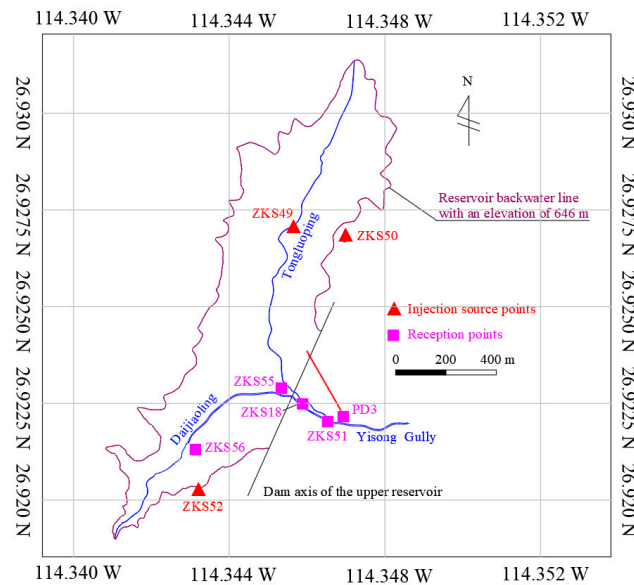


Figure 4. Location of the injection source and reception points for tracer tests in the upper reservoir.

Table 1. Summary of tracer test process.

Number of Tests	Test Time	Test Purpose	Injection Points	Reception Points	Detailed Description of the Test Process
Group 1	9:40 April 29 to 8:30 1 May 2023	Hydraulic connection between groundwater in the right bank and near the dam site	ZKS52	ZKS55, ZKS56, ZKS18, ZKS51, PD3	The salt tracer comprises 40 kg dissolved in 360 L of water, and the injection time is 10 min. Five reception points are automatically monitored with a measuring frequency of 1 min per time.
Group 2	10:46 May 1 to 8:30 4 May 2023	Hydraulic connection between groundwater within the reservoir and near the dam site	ZKS49	ZKS55, ZKS18, ZKS51, PD3	The salt tracer comprises 51 kg dissolved in 500 L of water, and the injection time is 10 min. Four reception points are automatically monitored with a measuring frequency of 1 min per time.
Group 3	10:19 May 8 to 8:20 10 May 2023	Hydraulic connection between groundwater on the left bank and near the dam site	ZKS50	ZKS18, ZKS49, ZKS51, ZKS55, PD3	The salt tracer comprises 10 kg dissolved in 75 L of water, and the injection time is 21 min. Five reception points are automatically monitored with a measuring frequency of 1 min per time.

4. Results

4.1. Identification of Multiple Leakage Paths in Complex Fracture Networks

The tracer test was conducted from 9:40 on 29 April 2023 to 8:30 on 1 May 2023. The injection point of the tracer was ZKS52 with an elevation of 656 m. There are five reception points, namely ZKS18, ZKS51, ZKS55, ZKS56, and PD3 (Figure 4). The results of conductivity over time at reception points are shown in Figure 5.

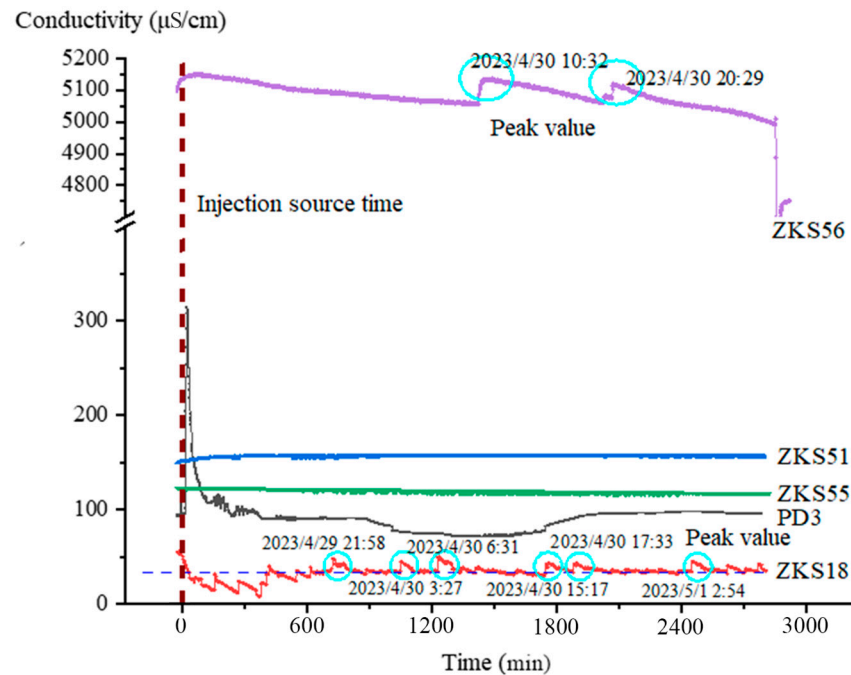


Figure 5. Relationship between conductivity and time at the reception points for the injection source of ZKS52.

It can be seen from Figure 5 that the conductivity of ZKS18 fluctuated irregularly after the tracer was injected, and did not exceed the background value of conductivity. After 12.2 h, the conductivity began to show a clear breakthrough curve with a total of six obvious peaks during the entire test period. The tracer was received in ZKS18 at 21:52 on 29 April. The conductivity exceeded $34.9 \mu\text{S}/\text{cm}$ and reached the first peak of $47.8 \mu\text{S}/\text{cm}$ at 21:58, and then the conductivity gradually decreased. On 30 April at 3:12, the conductivity reached the second peak of $44.7 \mu\text{S}/\text{cm}$ at 3:27, and the conductivity gradually decreased thereafter. The conductivity exceeded $34.8 \mu\text{S}/\text{cm}$ and reached the third peak of $49.6 \mu\text{S}/\text{cm}$ at 6:31 on 30 April. At 15:17 on 30 April, the conductivity reached the fourth peak of $43.9 \mu\text{S}/\text{cm}$. At 17:33 on 30 April, the conductivity reached the fifth peak of $43.1 \mu\text{S}/\text{cm}$, and at 2:48 on 1 May, the conductivity reached the sixth peak of $45.4 \mu\text{S}/\text{cm}$. It can be inferred that the tracer from ZKS52 was received in ZKS18, and there may be multiple leakage passages. Due to the fact that ZKS18 is pressurized water and the water level at the drilling site is higher than the surface, there may be multiple leakage points in ZKS18, which results in multiple peaks. According to Equations (2)–(4), the groundwater flow rates for the six leakage passages are 0.499 m/min, 0.343 m/min, 0.294 m/min, 0.208 m/min, 0.192 m/min, and 0.148 m/min, respectively. The difference in groundwater level between ZKS18 and ZKS52 is about 64.74 m, so the hydraulic gradient is 0.177. The permeability coefficients of the six main leakage passages are 2.819 m/min, 1.936 m/min, 1.66 m/min, 1.174 m/min, 1.087 m/min, and 0.837 m/min, respectively. Therefore, the calculated sizes of the six main leakage passages are 0.267 mm, 0.221 mm, 0.205 mm, 0.172 mm, 0.166 mm, and 0.145 mm, respectively.

The background value of the conductivity for ZKS56 is relatively high, which may be due to the short completion time of the hole, incomplete well washing, and certain contamination of groundwater in the hole. During the tracer test, we considered the relative conductivity, so high background values do not affect the results of the tracer test. A rapid increase in conductivity was seen within 20 min after the tracer was injected, and a slow decrease within the next 24 h. Therefore, the background value of conductivity is about $5060 \mu\text{S}/\text{cm}$. After injecting the tracer from 9:40 to 9:50 on 29 April, the tracer was received at ZKS56 at 9:41 on 30 April. The conductivity exceeded $5054.1 \mu\text{S}/\text{cm}$ and reached the first peak of $5136.2 \mu\text{S}/\text{cm}$ at 10:32. On 30 April at 19:42, the conductivity reached the

second peak of 5121.2 $\mu\text{S}/\text{cm}$ at 20:29, and then the conductivity gradually decreased and remained stable overall. Two obvious breakthrough curves appeared after 24 h and 34 h, which indicates that ZKS56 received the tracer from ZKS52, and there may be two main leakage passages.

The receipt of the tracers at ZKS18 and ZKS56 indicates the possible fracture or fault passages between ZKS18, ZKS56, and ZKS52. The groundwater flow direction is from ZKS52 to ZKS18 and ZKS56, which also indicates that there is a hydraulic connection between the groundwater on the right bank of the upper reservoir and at the bottom of the Yisonggou Gully. The groundwater on the right bank recharges the water in the Yisonggou Gully. At the same time, there is a hydraulic connection between the groundwater on the right bank of the reservoir and the bottom of the Dajiaoling Gully, and the groundwater on the right bank recharges the water of the Dajiaoling Gully.

The conductivity of ZKS51 and ZKS55 remained unchanged during the entire test, which indicates that no tracer was received. The conductivity of PD3 increased rapidly within half an hour after the tracer injection, then decreased rapidly and showed a clear breakthrough curve. However, based on on-site shooting records and analysis of temperature changes at PD3 monitoring points, PD3 fired around 10 o'clock that day, which is consistent with the time of the peak. At the same time as the peak appeared, the water temperature at the PD3 also increased. Therefore, it is inferred that the breakthrough curve of PD3 may have been formed due to the influence of blasting during tunnel construction.

4.2. Estimation of Hydrogeological Parameters and Leakage Passage Size for Rock Mass

The tracer test was conducted from 10:46 on 1 May 2023 to 8:30 on 4 May 2023, with the injection point of ZKS49 at an elevation of 584 m. There were four reception points, namely ZKS18, ZKS51, ZKS55, and PD3 (Figure 4). The results of conductivity changes over time at five monitoring points are shown in Figure 6.

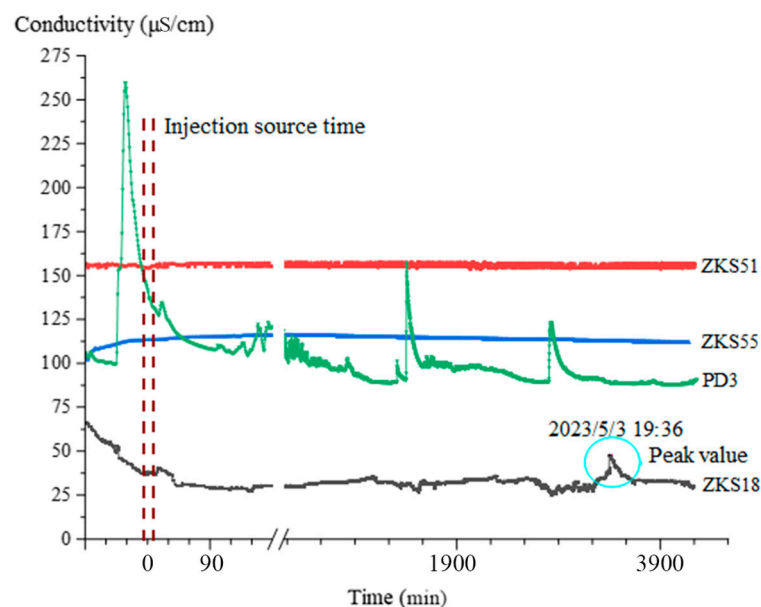


Figure 6. Relationship between conductivity and time at the reception points for the injection source point of ZKS49.

It can be seen from Figure 6 that the conductivity of ZKS18 showed irregular fluctuations after the tracer was injected, and basically did not exceed the background value of conductivity. After 54.2 h, the conductivity began to show a clear breakthrough curve. The tracer was received at ZKS18 at 16:59 on 3 May with a conductivity exceeding 30.9 $\mu\text{S}/\text{cm}$, reaching a peak of 47.6 $\mu\text{S}/\text{cm}$ at 19:36. Then the conductivity gradually decreased and remained relatively stable. It can be inferred that the tracer from ZKS49 was received at

ZKS18. Because the well screen at ZKS49 is arranged in the stratigraphic section exposed by the fully weathered interlayer QJ₂ (56–69 m), ZKS18 also exposed the fully weathered interlayer QJ₂ at the depth of 80 m. Therefore, it can be inferred that the tracer at ZKS49 was received through the leakage of the fully weathered interlayer QJ₂ layer by layer. Due to the long reception time, the hydraulic connection of the fully weathered interlayer QJ₂ is relative weak. The direction of groundwater flow is from ZKS49 to ZKS18 through the fully weathered interlayer QJ₂.

The receipt of the tracer at ZKS18 and the location of exposed strata indicate the presence of a completely weathered interlayer QJ₂ between ZKS18 and ZKS49. The size of the leakage passage can be estimated by the migration time of the tracer, the distance, and the groundwater level difference between the source and reception points. The distance between ZKS18 and ZKS49 is approximately 457.01 m. The migration time is 3253 min, so the groundwater flow rate is 0.14 m/min. The groundwater level difference between ZKS18 and ZKS49 is about 11.55 m, so the hydraulic gradient is 0.025 and the permeability coefficient is 5.559 m/min. According to Equation (4), the size of the leakage passage is calculated to be 0.375 mm.

The conductivities of ZKS51 and ZKS55 remained basically unchanged during the entire test, which indicates that no tracer was received. The conductivity of PD3 showed three significant peaks after the tracer was injected. However, based on the on-site records of PD3 blasting in the adit and the analysis of temperature changes at PD3 monitoring points, PD3 was fired around 11:30 noon on 1 May, 10:00 a.m. on 2 May, and 10:30 a.m. on 3 May, which was consistent with the peak time. At the same time, the water temperature at PD3 also increased. Therefore, it is inferred that the three breakthrough curves of PD3 in this test may have been formed due to the influence of blasting during the tunnel construction.

4.3. Determination of the Relationship between Groundwater Recharge, Runoff, and Discharge

The tracer test was conducted from 10:19 on 8 May to 8:20 on 10 May 2023 with the injection source point of ZKS50 and the elevation of 658 m. There were five reception points, namely ZKS18, ZKS49, ZKS51, ZKS55, and PD3 (Figure 4). The results of the conductivity changes over time at the five monitoring points are shown in Figure 7.

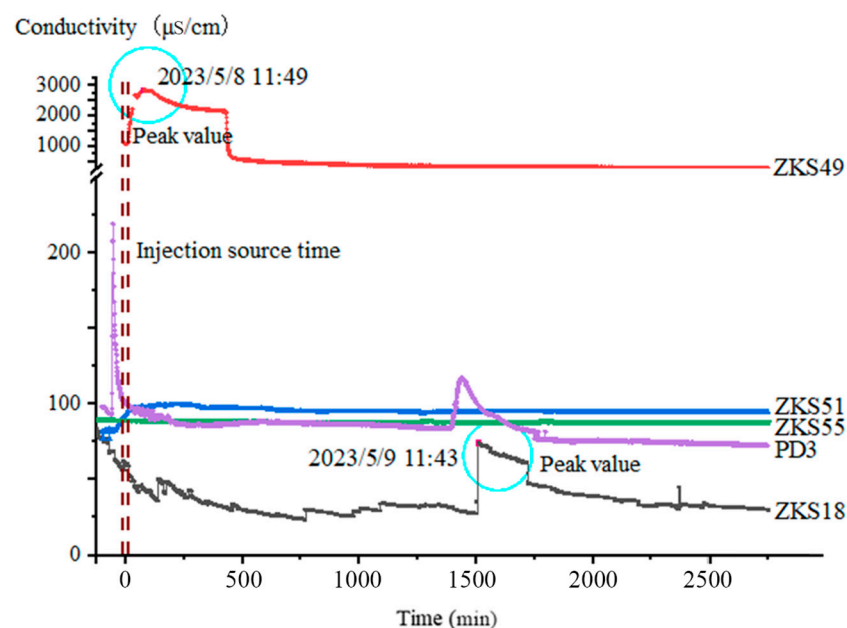


Figure 7. Relationship between conductivity and time at the reception points for the injection source point of ZKS50.

It can be seen from Figure 7 that the conductivity of ZKS18 fluctuates irregularly after the tracer was injected. After 25.3 h, the conductivity begins to show a clear breakthrough curve with a total of one obvious peak during the entire test period. The conductivity results showed that from 10:19 to 10:40 on 8 May, the tracer began to be received at ZKS18 at 11:35 on 9 May, and it reached a peak of 73.6 $\mu\text{S}/\text{cm}$ at 11:43; thereafter, the conductivity gradually decreased and remained stable, which indicates that a tracer from ZKS50 was received at ZKS18. The distance between ZKS18 and ZKS50 is approximately 447.16 m with a reception time of 1516 min, resulting in a groundwater flow rate of 0.295 m/min. The groundwater level difference between ZKS18 and ZKS50 is about 30.07 m, so the hydraulic gradient is 0.067 and the permeability coefficient is 4.386 m/min. The size of the leakage passage can be calculated as 0.333 mm based on Equation (4).

Due to the flow rate test conducted in ZKS49 on 8 May from 9 am to 11 am, during the tracer test, the initial conductivity value of ZKS49 was much higher than that of the other four reception points. When conducting a tracer test, the conductivity of ZKS49 slowly decreased. After 15 min, the conductivity value began to rapidly increase, reached its peak, and showed a clear breakthrough curve. On 8 May, after the tracer was injected at ZKS50, the tracer began to be received at ZKS49 at 10:34, and the conductivity reached a peak of 2829 $\mu\text{S}/\text{cm}$ at 11:49. It can be inferred that a tracer from ZKS50 was received at ZKS49. The above analysis indicates that the direction of groundwater flow is from ZKS50 to ZKS18 and ZKS49, which implies that there is a hydraulic connection between the groundwater on the left bank of the reservoir and the groundwater in Yisonggou and Tongluoping Gullies.

The conductivities of ZKS51 and ZKS55 remained basically unchanged during the entire test, which indicates that no tracer was received. The conductivity of PD3 rapidly increased to its peak after 24.3 h, and then rapidly decreased, which shows a clear breakthrough curve. However, according to on-site shooting records and analysis of temperature changes at PD3 monitoring points, PD3 fired around 9 a.m. on 9 May, which was consistent with the time of peak occurrence. At the same time, as the peak appeared, the water temperature at PD3 also increased. Therefore, it is inferred that the breakthrough curve of PD3 in this test may have been formed by the influence of firing.

Based on the above analysis, the groundwater in the upper reservoir is mainly discharged from the mountains on both banks to the bottom of the gullies. The groundwater on the left bank is mainly discharged towards the Tongluoping Gully, while the groundwater on the right bank is mainly discharged towards the Daijiaoling Gully, and finally converges and discharges towards the Yisong Gully. The mechanism of recharge and discharge near Tongluoping Gully is that rainfall infiltrates into the cover layer and bedrock, and forms a quantity of upper stagnant water in the cover layer. Some of the water in the cover layer recharges groundwater, while other water is directly discharged or exposed as spring water to recharge surface water. The water in the bedrock mainly recharges groundwater. Based on the groundwater levels of ZKS49, it can be seen that the water level at the bottom of Tongluoping Gully is significantly lower than that of the gully, and there is a 'disconnection' phenomenon between the gully water and groundwater. Therefore, the relationship between surface water and groundwater at the bottom of Tongluoping Gully is that surface water recharges groundwater. The relationship near Yisong Gully is that rainfall infiltrates into the cover layer and bedrock, and forms upper stagnant water in the cover layer. Part of the water in the cover layer recharges groundwater, while the other water directly recharges surface water. Due to the exposure of three layers of soluble rock formations at the dam foundation, and considering the relatively low permeability of the fully weathered interlayer QJ₂, which serves as a relatively impermeable layer, there are at least two confined aquifers in the Yisong Gully dam site area. These mainly receive recharge from rainfall and groundwater from the mountains on both banks, and discharge into the groundwater and surface water.

4.4. Determination of Groundwater Flow Rate and Direction

Single-hole tracer tests were conducted on boreholes ZKS49, ZKS50, ZKS52, and ZKS55 (Figure 4). Three different depths were determined for each test hole, and a total of 12 sets of tests were conducted. The calculation results are shown in Table 2. It can be seen from Table 2 that as the depth increases, the groundwater flow rate increases. Among them, borehole ZKS49 has a significant difference in the direction of groundwater flow at different depths, while the other boreholes have little difference in the direction of groundwater flow at different depths. This may be due to the presence of fractures or faults in the test sections, which causes the local groundwater flow direction to be inconsistent with the overall groundwater flow direction. The groundwater flow rate and direction calculated by the vector synthesis method are basically consistent with that using the three-hole method, which indicates that the vector synthesis method in the single hole can be used for determining the flow rate and direction of groundwater flow.

Table 2. Calculated results of groundwater flow rate and direction.

Borehole Number	Borehole Location	Test Depth (m)	Vector Synthesis Method		Three-Hole Method	
			Groundwater Flow Direction (°)	Groundwater Flow Rate (m/d)	Groundwater Flow Direction (°)	Groundwater Flow Rate (m/d)
ZKS49	Tongluoping Gully	25	252.4	4.95	259	4.79
		56	135.6	9.42	/	/
		65	142.3	9.88	/	/
ZKS50	Left bank	75	260.5	3.25	258	3.18
		90	263.2	5.12	/	/
		110	258.4	6.89	/	/
ZKS52	Right bank	45	353.6	6.83	355	6.59
		70	358.5	7.15	/	/
		85	356.3	7.34	/	/
ZKS55	Yisong Gully	2	122.5	2.85	125	2.76
		35	135.6	12.65	/	/
		70	126.8	15.47	/	/

5. Conclusions

Tracer tests are commonly used to identify the complex hydrogeological conditions in fractured rocks. This study conducted three sets of tracer tests and multiple sets of single-hole flow rate and direction tests, and obtained the following conclusions:

- (1) The reception point ZKS18 received tracers from three sets of tracer tests, which indicates that the groundwater in the dam site area mainly comes from the recharge of the mountains on both banks. The tracer injection well for the second group of tests is located in Tongluoping Gully within the reservoir. After the reservoir is filled with water, there is a possibility of leakage from inside to outside the reservoir.
- (2) The results of the tracer tests showed that there were one or more conductivity peaks at the tracer reception points, which indicates the existence of multiple leakage passages between the injection and the reception points. Based on the theory of groundwater dynamics, some hydrogeological parameters, such as flow rate, hydraulic gradient, and permeability coefficient, were calculated, and it was determined that there were 1–6 leakage passages in the study area with a leakage passage size of 0.1–0.4 mm.
- (3) According to the tests of the single-hole flow rate and direction, a conductivity monitoring instrument was independently developed, and a new method for determining groundwater flow rate and direction was proposed. The flow rate and direction determined by the proposed method are basically consistent with those of the three-hole

method, which indicates that the proposed method is effective and reliable, and can be used to identify groundwater leakage passages. The method provides a reliable basis for subsequent anti-seepage design and leakage reinforcement.

Author Contributions: Conceptualization, W.C.; methodology, W.C. and J.Z.; validation, J.Z., L.C., X.D. and Y.H.; formal analysis, W.C. and J.Z.; resources, W.C. and Y.H.; data curation, J.Z., K.M., L.C. and Y.H.; writing—original draft preparation, W.C.; writing—review and editing, J.Z., K.M. and X.D.; supervision, W.C., L.C. and Y.H.; project administration, L.C. and Y.H.; All authors have read and agreed to the published version of the manuscript.

Funding: This research was funded by the National Natural Science Foundation of China Joint Fund Project, grant number U2240217.

Data Availability Statement: Data are contained within the article.

Acknowledgments: The authors would like to acknowledge the financial support from the National Natural Science Foundation of China Joint Fund Project. The authors would also like to thank the School of Earth Sciences and Engineering at Hohai University for partial support of the graduate student on this project.

Conflicts of Interest: Author Wanlin Chen was employed by the company Huadong Engineering (Fujian) Corporation Limited. Author Liqiang Chen was employed by the company PowerChina Huadong Engineering Corporation Limited. The remaining authors declare that the research was conducted in the absence of any commercial or financial relationships that could be construed as a potential conflict of interest.

References

- Li, G.; Han, Z. Principal Engineering Geological Problems in the Shisanling Pumped Storage Power Station, China. *Eng. Geol.* **2004**, *76*, 165–176. [[CrossRef](#)]
- Li, P.; Lu, W.; Long, Y.; Yang, Z.; Li, J. Seepage Analysis in a Fractured Rock Mass: The Upper Reservoir of Pushihe Pumped-Storage Power Station in China. *Eng. Geol.* **2008**, *97*, 53–62. [[CrossRef](#)]
- Miao, K.; Bai, Z.; Huang, Y.; Huang, Y.; Su, Y. Research on Seepage Control of Jurong Pumped Storage Hydroelectric Power Station. *Water* **2022**, *14*, 141. [[CrossRef](#)]
- Zhang, W.; Shen, Z.; Chen, G.; Zhang, W.; Xu, L.; Ren, J.; Wang, F. Optimization Design and Assessment of the Effect of Seepage Control at Reservoir Sites under Karst Conditions: A Case Study in Anhui Province, China. *Hydrogeol. J.* **2021**, *29*, 1831–1855. [[CrossRef](#)]
- Lu, X.; Wang, W.; Luo, C.; Wu, M.; Yang, C.; Liao, X.; Liu, L.; Fu, Z. A Rapid Detection Method of Towed Array Seismic Surface Wave for Leakage Passage of Dyke-Dam. *J. Appl. Geophys.* **2023**, *217*, 105189. [[CrossRef](#)]
- Sukanya, S.; Noble, J.; Joseph, S. Application of Radon (^{222}Rn) as an Environmental Tracer in Hydrogeological and Geological Investigations: An Overview. *Chemosphere* **2022**, *303*, 135141. [[CrossRef](#)] [[PubMed](#)]
- Liu, B.; Wang, C.; Liu, Z.; Xu, Z.; Nie, L.; Pang, Y.; Wang, N.; Feng, S. Cascade Surface and Borehole Geophysical Investigation for Water Leakage: A Case Study of the Dehou Reservoir, China. *Eng. Geol.* **2021**, *294*, 106364. [[CrossRef](#)]
- Meng, Y.; Fang, Y.; Wan, M.; Su, Q.; Tian, B.; Tong, F. Research of Concrete Dam Leakage Detection Based on Anomaly Current Field of Reservoir Water. *J. Appl. Geophys.* **2019**, *160*, 242–253. [[CrossRef](#)]
- Kana, J.D.; Djongyang, N.; Zakari, A.; Kasi, N.; Raïdandi, D.; Nouck, P.N.; Assastsé, W.T.; Tabod, T.C. GIS Based Exploring of Low-Enthalpy Geo-Energy Potentials in the Subsaharan Area in Central Africa. *Geomech. Geophys. Geo-Energy Geo-Resour.* **2021**, *7*, 94. [[CrossRef](#)]
- Huang, Y.; Zhou, Z.; Wang, J.; Chen, Z. Investigation of the Hydraulic Connection between the Upper Storage Reservoir and the Underground Powerhouse in the Hongping Pumped Storage Hydroelectric Powerstation. *Environ. Earth Sci.* **2018**, *77*, 193. [[CrossRef](#)]
- Xu, X.; Zeng, Q.; Li, D.; Wu, J.; Wu, X.; Shen, J. GPR Detection of Several Common Subsurface Voids inside Dikes and Dams. *Eng. Geol.* **2010**, *111*, 31–42. [[CrossRef](#)]
- Cen, X.; Xu, M.; Qi, J.; Zhang, Q.; Shi, H. Characterization of Karst Conduits by Tracer Tests for an Artificial Recharge Scheme. *Hydrogeol. J.* **2021**, *29*, 2381–2396. [[CrossRef](#)]
- Zhang, Y.; Huang, T. DNA-Based Tracers for the Characterization of Hydrogeological Systems—Recent Advances and New Frontiers. *Water* **2022**, *14*, 3545. [[CrossRef](#)]
- Lorenzi, V.; Banzato, F.; Barberio, M.D.; Goeppert, N.; Goldscheider, N.; Gori, F.; Lacchini, A.; Manetta, M.; Medici, G.; Rusi, S.; et al. Tracking Flowpaths in a Complex Karst System through Tracer Test and Hydrogeochemical Monitoring: Implications for Groundwater Protection (Gran Sasso, Italy). *Heliyon* **2024**, *10*, e24663. [[CrossRef](#)] [[PubMed](#)]

15. Aquilanti, L.; Clementi, F.; Nanni, T.; Palpacelli, S.; Tazioli, A.; Vivalda, P.M. DNA and Fluorescein Tracer Tests to Study the Recharge, Groundwater Flowpath and Hydraulic Contact of Aquifers in the Umbria-Marche Limestone Ridge (Central Apennines, Italy). *Environ. Earth Sci.* **2016**, *75*, 626. [[CrossRef](#)]
16. Bodin, J.; Porel, G.; Nauleau, B.; Paquet, D. Delineation of Discrete Conduit Networks in Karst Aquifers via Combined Analysis of Tracer Tests and Geophysical Data. *Hydrol. Earth Syst. Sci.* **2022**, *26*, 1713–1726. [[CrossRef](#)]
17. Nanni, T.; Vivalda, P.M.; Palpacelli, S.; Marcellini, M.; Tazioli, A. Groundwater Circulation and Earthquake-Related Changes in Hydrogeological Karst Environments: A Case Study of the Sibillini Mountains (Central Italy) Involving Artificial Tracers. *Hydrogeol. J.* **2020**, *28*, 2409–2428. [[CrossRef](#)]
18. Martín-Rodríguez, J.F.; Mudarra, M.; De la Torre, B.; Andreo, B. Towards a Better Understanding of Time-Lags in Karst Aquifers by Combining Hydrological Analysis Tools and Dye Tracer Tests. Application to a Binary Karst Aquifer in Southern Spain. *J. Hydrol.* **2023**, *621*, 129643. [[CrossRef](#)]
19. Ren, K.; Pan, X.; Peng, C.; Chen, J.; Li, J.; Zeng, J. Tracking Contaminants in Groundwater Flowing across a River Bottom within a Complex Karst System: Clues from Hydrochemistry, Stable Isotopes, and Tracer Tests. *J. Environ. Manag.* **2023**, *342*, 118099. [[CrossRef](#)] [[PubMed](#)]
20. Qiu, H.; Hu, R.; Huang, Y.; Gwenzi, W. Detection and Quantification of Dam Leakages Based on Tracer Tests: A Field Case Study. *Water* **2022**, *14*, 1448. [[CrossRef](#)]
21. Hua, C.; Jiang, Z.; Li, J.; Xu, T.; Lei, Y.; Zhu, H. Tracer-Test-Based Dimensionality Reduction Model for Characterizing Fracture Network and Predicting Flow and Transport in Fracture Aquifer. *J. Hydrol.* **2024**, *630*, 130773. [[CrossRef](#)]
22. Dogančić, D.; Afrasiabian, A.; Kranjčić, N.; Đurin, B. Using Stable Isotope Analysis (δD and $\delta 18O$) and Tracing Tests to Characterize the Regional Hydrogeological Characteristics of Kazeroon County, Iran. *Water* **2020**, *12*, 2487. [[CrossRef](#)]
23. Agbotui, P.Y.; West, L.J.; Bottrell, S.H. Characterisation of Fractured Carbonate Aquifers Using Ambient Borehole Dilution Tests. *J. Hydrol.* **2020**, *589*, 125191. [[CrossRef](#)]
24. Fahrmeier, N.; Goeppert, N.; Goldscheider, N. Comparative Application and Optimization of Different Single-Borehole Dilution Test Techniques. *Hydrogeol. J.* **2021**, *29*, 199–211. [[CrossRef](#)]
25. Façanha, J.M.F.; Maqueira, L.; Souza, A.V.O.; Moura, P.G.; Pérez-Gramatges, A. Conservative Tracer Tests in Sandstones and Carbonates Using a Cost-Effective Fluorescence Method. *J. Pet. Sci. Eng.* **2020**, *195*, 107764. [[CrossRef](#)]
26. Pitrak, M.; Mares, S.; Kobr, M. A Simple Borehole Dilution Technique in Measuring Horizontal Ground Water Flow. *Groundwater* **2007**, *45*, 89–92. [[CrossRef](#)] [[PubMed](#)]
27. Zhou, Z.F. *Theory on Dynamics of Fluids in Fractured Medium*, 2nd ed.; Geological Publishing House: Beijing, China, 2019; pp. 15–31.

Disclaimer/Publisher’s Note: The statements, opinions and data contained in all publications are solely those of the individual author(s) and contributor(s) and not of MDPI and/or the editor(s). MDPI and/or the editor(s) disclaim responsibility for any injury to people or property resulting from any ideas, methods, instructions or products referred to in the content.